Compact Constant Mean Curvature Surfaces with Low Genus

Karsten Große-Brauckmann and Konrad Polthier

CONTENTS

We describe numerical experiments that suggest the existence of certain new compact surfaces of constant mean curvature. They come in three dihedrally symmetric families, with genus ranging from 3 to 5, 7 to 10, and 3 to 9, respectively; there are further surfaces with the symmetry of the Platonic polyhedra and genera 6, 12, and 30. We use the algorithm of Oberknapp and Polthier, which defines a discrete version of Lawson's conjugate surface method.

INTRODUCTION

Surfaces with constant mean curvature have been studied for a long time. Until recently most known boundaryless or complete surfaces were minimal, that is, had mean curvature $H = 0$; the only surfaces with nonzero constant H were Delaunay's surfaces of revolution [1841]. Compact surfaces have attracted particular attention. The maximum principle rules out the existence of compact minimal surfaces, but for $H \neq 0$ the case is altered, and some constructions are now known. As we describe below, the resulting compact surfaces are rather complicated and also not quite as explicit as one might hope. In the present work we compute surfaces that are geometrically simpler: they are small and have a large symmetry group.

Assume H is a nonzero constant and normalize it to 1 by a scaling; we use the shorthand notation CMC for this case. The simplest compact CMC surface is the unit sphere. The sphere is known as the unique embedded CMC surface [Aleksandrov 1958], and also the unique immersed CMC sphere [Hopf 1983]. Both results focused much attention

Große-Brauckmann was supported by SFB 288 at Technische Universität Berlin and SFB 256 at Universität Bonn.

Polthier was partially supported by SFB 288 at Technische Universität Berlin.

AMS Subject Classification: 53A10.

1058-6458/97 $0.50 per page

on the existence problem for further compact CMC surfaces. It is also interesting that the sphere is the only complete CMC surface that is a minimum for the variational problem for constant mean curvature [Barbosa and do Carmo 1984]: find critical levels of area for a given enclosed volume. The partial differential equation $H =$ constant can be considered the Euler equation to the variational problem.

Wente's existence proof for CMC tori [1986] was a surprising event and triggered further discoveries. Pinkall and Sterling [1989] characterize all immersions that cover CMC tori, and Bobenko [1991] gives explicit formulae for their induced metrics in terms of theta functions. These immersions lead to compact CMC tori only if all periods vanish, otherwise to noncompact periodic surfaces. It is known that the period condition is in fact satisfied in some cases [Ercolani et al. 1993]. In his numerical work Heil [1995] evaluates the theta functions and studies the period problem.

Kapouleas [1991] constructs a large class of compact CMC surfaces for every genus $g \geq 3$. He glues pieces of Delaunay surfaces onto spheres and proves existence of nearby smooth CMC surfaces by an implicit function theorem argument. The Delaunay pieces must be long, and all neck sizes tiny—how long and how thin precisely is the result of delicate estimates and hence practically not accessible. In [Kapouleas 1995] surfaces of every genus $g \geq 2$ are constructed using g Wente tori that are glued together at a single lobe. Similar to the case of Kapouleas' Delaunay-like surfaces the fused Wente tori are almost degenerate: they have a large number of almost spherical lobes joined by necks of large Gauß curvature.

We use the algorithm of Oberknapp and Polthier [1997] to construct compact surfaces numerically. This algorithm gives a discrete version of the conjugate surface construction introduced by Lawson [1970]. Lawson constructed two doubly periodic CMC surfaces with his method. Many other complete surfaces, both periodic and of finite topology, have been constructed by Karcher [1989] and Große-Brauckmann [1993] using extensions of the conjugate surface method.

The conjugate surface method of Lawson generates symmetric surfaces by planar reflection from a simply connected fundamental domain. For all our surfaces this domain is bounded by five planar arcs and depends on two parameters. On the other hand there are two period conditions to satisfy. To solve these two period problems rigorously is a serious problem for our domains (see 2), and this is the main reason why we must rely on a numerical method. All other steps in our existence program can be theoretically proved similar to the noncompact examples constructed in [Große-Brauckmann 1993].

Here we complete the studies begun with the three examples of [Große-Brauckmann and Polthier 1996] in the sense that we determine maximal families of similar surfaces; the surfaces are isolated and the families are finite. Our three previous surfaces were chosen rather close to the degenerate spherical situation, i.e., with thin necks, so that existence could be expected from Kapouleas' work [1991] but not predicted. Most surfaces we present now have large necks. Thus they are further away from Kapouleas' class of surfaces, and they are also numerically easier to deal with.

In a way made precise in Section 4B our surfaces can be characterized by an underlying graph consisting of edges and vertices. Spheres or k-fold necks are located at the vertices, and one Delaunay neck on each edge of the graph. Our CMC surfaces have the symmetry of the underlying graph. These symmetries are given by discrete subgroups of $O(3)$ generated by reflections: we have examples with dihedral symmetry and with the symmetry group of the Platonic polyhedra.

What considerations guided our search for CMC surfaces, and what further surfaces can be expected to exist? There are necessary conditions to satisfy: most important is Kusner's balancing formula discussed in Section 4. We view this condition as a condition on the edge length of the underlying graph. Furthermore, the Delaunay surfaces

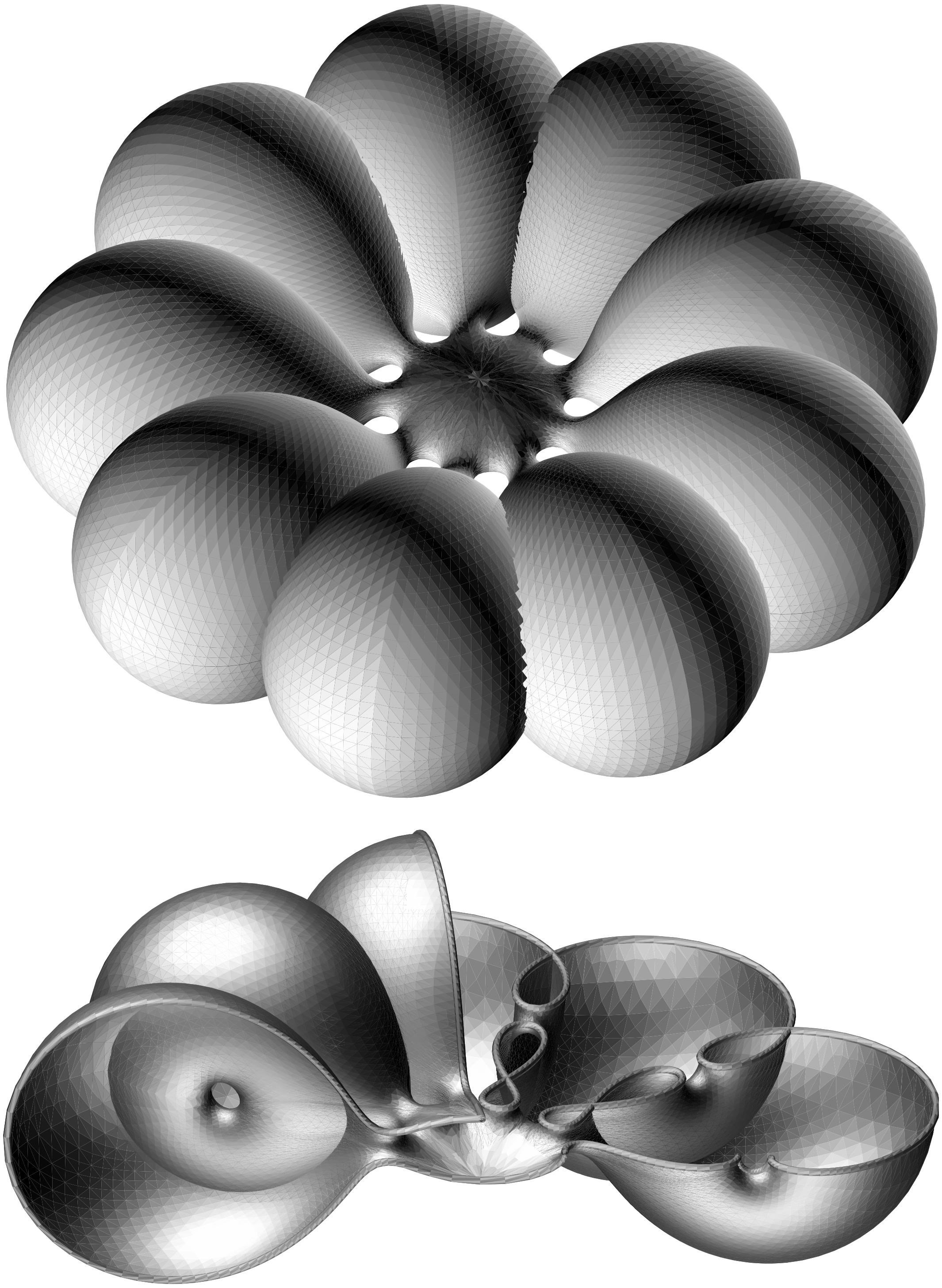

FIGURE 1. Top: A dihedrally symmetric noidal surface of genus 9. We call the central 9-fold junction noidal because it is related to the minimal 9-noid. We find similar surfaces for all genera from 3 to 9. Bottom: Part of the same surface with a view of the nodoidal necks connecting adjacent outer bubbles. The boundary is thickened with small tubes.

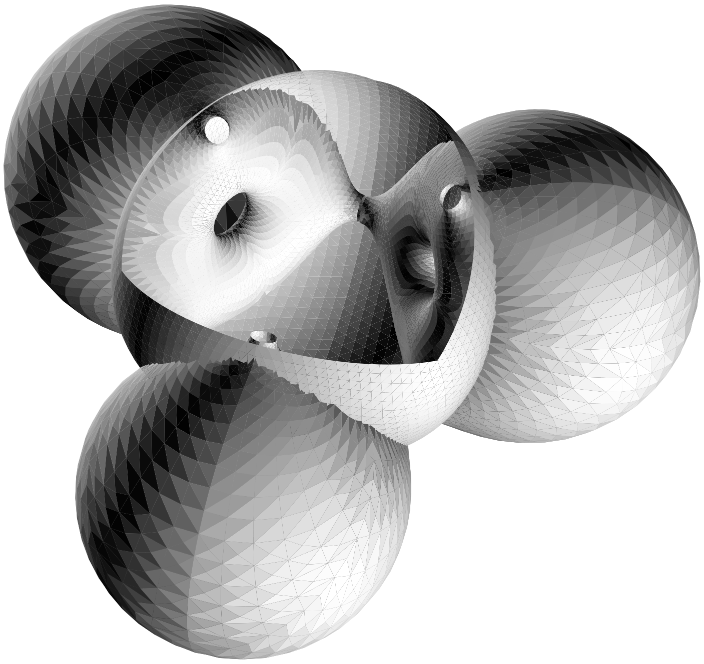

FIGURE 2. A surface of genus 6 with the symmetry of a tetrahedron. One bubble is removed. Six unduloidal necks join the four outer bubbles pairwise. The central bubble looks like a shell punctured in four points to connect it nodoidally to each outer bubble.

and their k-end dihedrally symmetric generalizations (Section 5) indicate that further constraints beyond those given by the balancing formula are present. In particular a comparison with these surfaces leads to an explanation why our families only range over finitely many genera.

The numerical algorithm of Oberknapp and Polthier generalizes an algorithm for discrete harmonic maps and minimal surfaces by Pinkall and Polthier [1993]. There are two steps: minimizing area (in fact discrete Dirichlet energy) in $\mathbb{S}^3$, and conjugating the discrete surface to a CMC surface in $\mathbb{R}^3$. The algorithm is implemented as part of the graphical environment GRAPE developed by the Sonderforschungsbereich 256 at the University of Bonn. The algorithm works with discrete data, and we cannot estimate how close the resulting polyhedral surfaces are to smooth CMC surfaces. Although we are confident that we correctly determined the range of genera for which our types of surfaces exist, some care is appropriate with regard to the exact shape of our surfaces. We hope future proofs will support our experimental results.

1. EXPERIMENTAL RESULTS

1A. Dihedrally Symmetric Surfaces

In Table 1 we summarize the class of surfaces with genus g and *dihedral symmetry group* $D_g \times \mathbb{Z}_2$. Slightly abusing notation we let this be the symmetry group of a planar regular g-gon considered as a subset of $\mathbb{R}^3$; the $\mathbb{Z}_2$-factor stands for reflection in the plane of the g-gon. $4g$ copies of a fundamental domain like the one shown in Figure 5 on page 19 combine to the entire compact surface. The symmetry groups also admit $4g$ fundamental cells in $\mathbb{R}^3$, shaped like cake slices; as will be clear from by Figure 5, such a cell does not contain an entire fundamental domain of the surface.

The soul of the surfaces is a planar graph G_g consisting of a regular g-gon with g additional edges (*spokes*) joining the midpoint to each vertex; see Figure 3. By the balancing formula (see Section 4A below) g must be at least 3. The graph G_g has only two independent lengths and we let its *length quotient* $q_g = 2\sin(\pi/g)$ be the quotient of the polygonal edge length over the length of the spokes.

For certain genera we obtain two different surfaces. These pairs are most clearly distinguished by the geometry of their centre in a way that is

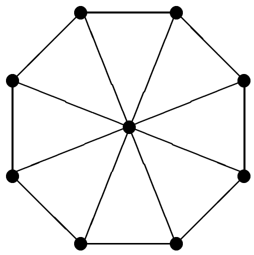

FIGURE 3. The underlying graph G_8 for the two genus 8 surfaces depicted in Figure 15. Vertices represent bubbles and edges necks.

genus g	centre	necks on spokes	necks on polygon	length quotient q_g	polygonal neck circumference	Figure
3				$1+0.73$	0.66	12
4		nodoidal	unduloidal	$1+0.41$	0.36	13
5				$1+0.18$	0.16	[GP1996]
(6)		(degenerate 7 spheres)		1	(0)	
7	spheroidal			$1-0.13$	not studied	
8				$1-0.23$	0.23	15, top
9		unduloidal	nodoidal	$1-0.32$	0.41	—
10				$1-0.38$	0.63	—
(≥ 11)				surfaces do not exist		
3				$2(1-0.13)$	0.07	[GP1996]
4				$2(1-0.29)$	0.21	14
5				$2(1-0.41)$	0.31	—
6	noidal	unduloidal	nodoidal	$2(1-0.5)$	not studied	
7				$2(1-0.57)$	not studied	
8				$2(1-0.62)$	0.65	15, bottom
9				$2(1-0.66)$	0.71	1
(≥ 10)				surfaces do not exist		

TABLE 1. Surfaces with dihedral symmetry $D_g \times \mathbb{Z}_2$, graph G_g and at most one neck per edge of the graph. [GP1996] stands for our previous paper [1996].

apparent from Figure 15. Furthermore, the type we call spheroidal has two different neck distributions that depend on the genus, in fact on the sign of $q_g - 1$. In the following sections we will make the terminology used in Table 1 more precise and explain this fact.

By their symmetry the dihedrally symmetric surfaces have umbilics on the two points contained in the vertical axis of rotation. Using the Gauß–Bonnet formula it can be shown there are no further umbilics.

In the following sections we will explain why the experimental existence of certain surfaces implies the existence of others. Hence it was not necessary to carry out experiments for all surface candidates, and we marked surfaces we could skip with "not studied" in our tables. In Table 1 we also include a degenerate CMC surface consisting of seven spheres with symmetry $D_6 \times \mathbb{Z}_2$. Since $q_6 = 1$ these spheres match in the sense that they touch tangentially on points of G_6.

Experimental Result 1.1. All of the fourteen dihedrally symmetric complete compact CMC surfaces listed in Table 1 exist. These are all the CMC surfaces with graph G_g and at most one neck per edge of the graph.

We would like to remark that the graphs G_g admit further surfaces with more than one neck per edge; in particular Kapouleas' construction [1991] applies to some large number of bubbles. Also, in Section 7 we suggest further graphs that could lead to dihedrally symmetric surfaces.

1B. Surfaces with Platonic symmetry

There are three singular discrete subgroups of $O(3)$, given by the symmetry groups of the Platonic polyhedra. These groups are generated by reflections and we call them *Platonic symmetry groups.* The graph consists of the edge graph of a Platonic polyhedron with further edges (spokes) joining the vertices to the centre of the polyhedron. We obtain

genus g	graph contains	centre	necks on spokes	necks on polyhedron	length quotient	polyhedral neck circumference	Figure
6	tetrahedron	spheroidal	nodoidal	unduloidal	$1+0.63$	0.48	2
12	cube				$1+0.15$	0.38	17
12	octahedron				$1+0.14$	0.33	—
30	icosahedron				$1+0.05$	0.2	[GP1996]
30	dodecahedron		unduloidal	nodoidal	$1-0.29$	not studied	
6	tetrahedron	noidal	unduloidal	nodoidal	$2(1-0.18)$	not studied	
12	cube				$2(1-0.42)$	0.25	16
12	octahedron				$2(1-0.43)$	not studied	
30	icosahedron				$2(1-0.53)$	0.15	—
(30)	dodecahedron				$2(1-0.64)$	surface does not exist	

TABLE 2. Surfaces with Platonic symmetry. The edges of the Platonic polyhedra with spokes to their centre form the graphs; the surfaces have at most one neck per edge.

surfaces whose geometry is similar to the dihedrally symmetric surfaces.

Experimental Result 1.2. The nine complete compact CMC surfaces with Platonic symmetry listed in Table 2 exist. The surface with noidal centre and graph derived from the dodecahedron does not exist with one neck per edge.

As in the planar case we let the length quotient be the edge length of the polyhedron inscribed to the unit sphere. It is not the length quotient alone but also the combinatorics of the polyhedron that influence the polyhedral neck size listed in Table 2.

The genus of the surfaces with Platonic symmetry is the number of handles attached to the central sphere, that is the number of edges of the polyhedron. The outermost point of each polyhedral bubble is umbilic, as well as further points on the central bubble.

2. THE CONJUGATE SURFACE CONSTRUCTION

The conjugate surface construction for CMC surfaces generalizes a similar construction for minimal surfaces. Lawson established a local relation of CMC surfaces in $\mathbb{R}^3$ and spherical minimal surfaces in $\mathbb{S}^3$:

Theorem 2.1 [Lawson 1970, p. 364]. (i) *For a simply connected minimal surface $M \subset \mathbb{S}^3$ there exists an isometric* CMC *surface $\tilde{M} \subset \mathbb{R}^3$ and vice versa.*
(ii) *Furthermore, M is bounded by a polygon Γ of great circle arcs in $\mathbb{S}^3$ if and only if $\tilde{M}$ is bounded by geodesic curvature lines.*

Suppose that a fundamental domain of a CMC surface with respect to a group of reflections is simply connected, and its boundary consists of piecewise planar geodesic curvature arcs. Then by (ii) the Plateau solution to a suitable great circle polygon in $\mathbb{S}^3$ can produce such a fundamental CMC domain, and this domain can then be reflected to a complete CMC surface. Which spherical polygon do we have to take? The angles $\pi/(k+1)$ (with $k \in \mathbb{N}$) at the vertices of the fundamental domain and the position of the normal at the vertices are needed to prescribe all angles of the spherical polygon. These data are immediate from the symmetry type of the fundamental CMC domain and determine the spherical polygon up to its lengths. In general a polygon with fixed angles and n edges has $n-3$ free parameters for the lengths. Not all lengths can be prescribed to any given value though. The set of lengths attained for a given set of angles can be determined using spherical trigonometry. The

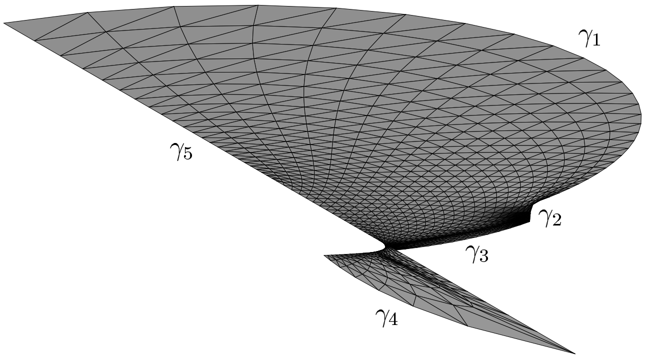

FIGURE 4. Fundamental domain for the spheroidal surface of genus 8 (see Figure 15). A polygon of five great circle arcs in $\mathbb{S}^3$ bounds the minimal surface patch. The patch is close to a great sphere $\mathbb{S}^2 \subset \mathbb{S}^3$, or, in the chosen stereographic projection, close to a plane. There are two helicoidal regions, one connecting the triangle to the two-gon, the other in a neighbourhood of γ_2.

construction is explained in more detail in [Lawson 1970; Karcher 1989; Große-Brauckmann 1993].

For two reasons the conjugate surface construction will only lead to sufficiently symmetric CMC surfaces: first, the fundamental domain must be simply connected; second, the theoretical or numerical Plateau solution we take is a stable minimizer, and thus the fundamental domain must be small enough to be stable [Große-Brauckmann and Polthier 1996, Section 4.2].

The period problem. The spherical boundary polygons we consider in the present work are pentagons. Thus our fundamental CMC domains are bounded by five planar arcs contained in five planes. Two pairs of planes are parallel by construction, and only if they coincide the surface generated by reflection is compact—otherwise the surface will be doubly periodic. We solve this *period problem* by adjusting the $5-3=2$ free parameters of the pentagon until the two pairs of planes coincide. Consequently our CMC surfaces are experimentally isolated.

In a more general sense all generators of the fundamental group give rise to periods. For our symmetric surfaces many of these periods agree; others,

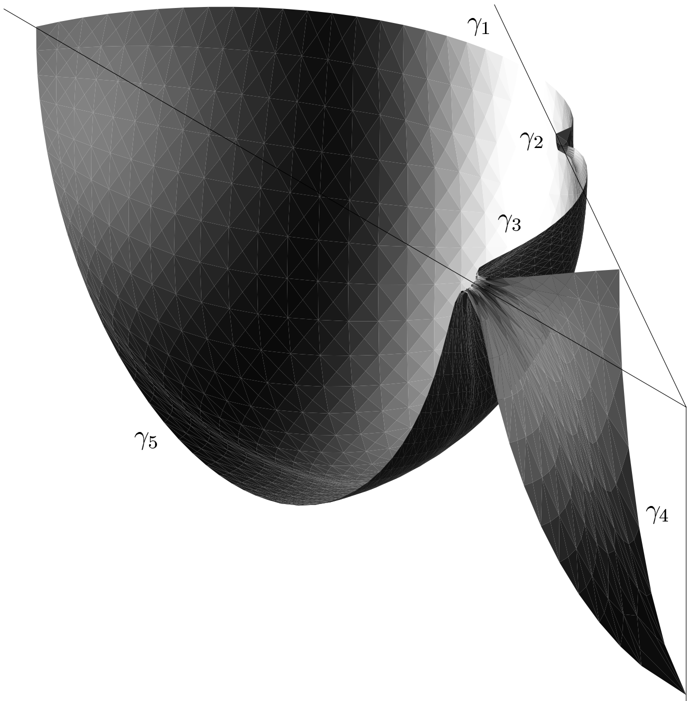

FIGURE 5. The isometric conjugate CMC patch. Its five boundary arcs are contained in three different planes that meet pairwise in the lines shown. Thirty-two reflected copies generate the compact surface depicted in Figure 15. The almost-planar regions of the previous figure give spherical regions whilst the helicoidal regions result in necks. These can be nodoidal (at γ_2), or unduloidal (in between γ_3 and γ_5) depending on the sense of rotation of the helicoids.

like the period of the unduloidal neck in Figure 6, are closed by symmetry. Thus the symmetry assumption reduces the number of different periods to two, regardless of the genus. Besides tori we do not know any compact surfaces that give rise to one period problem only. This makes two periods the simplest case to consider, while there are certainly many surfaces that pose three or more period problems.

To close the periods in a rigorous way one would have to give a loop in the parameter space so that the periods (viewed as a map to $\mathbb{R}^2$) can be estimated to have nonzero winding number about the origin. Then continuity of the family in its

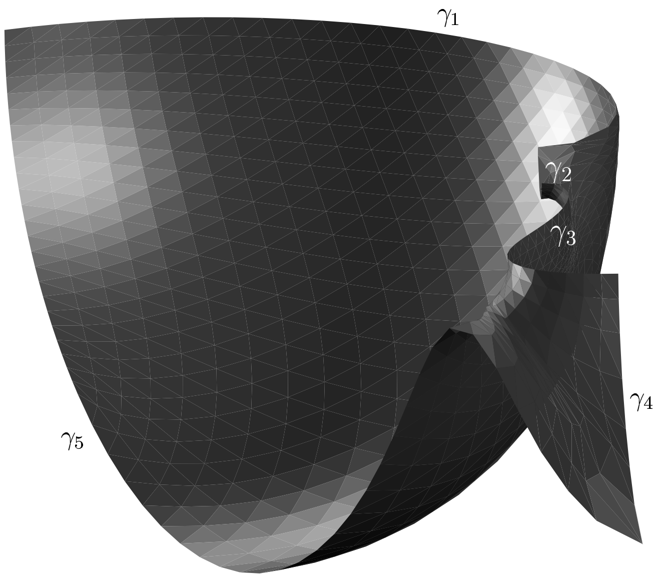

FIGURE 6. Period problem. The two-parameter family of patches gives rise to two periods: one is given by the distance between the vertical planes containing γ_2 and γ_4, the other between the horizontal planes containing γ_1 and γ_3. Unlike the previous figure the patch shown has nonzero periods so that repeated reflection results in a doubly periodic CMC surface.

parameters would imply the existence of a surface with 0 periods. Continuity of the surfaces is experimentally observed, however, it is difficult to prove. The standard proof is to recover a surface as graph; it fails in the example of the spherical domain depicted in Figure 4, since the two helicoidal regions are not graph with respect to any one direction.

3. THE ALGORITHM

Fundamental pieces of CMC surfaces are rarely stable if they are considered as a solution to a free boundary value problem, see [Große-Brauckmann and Polthier 1996] for a discussion. Hence only sufficiently small fundamental domains can be obtained by minimization of area under a volume constraint. A more general approach suggested by R. Kusner is to minimize the energy $\int (H-1)^2$; this can be done [Große-Brauckmann 1997] with the Surface Evolver [Brakke 1992]. At present the compact surfaces of this paper seem out of reach for that approach.

Generalizing the algorithm of Pinkall and Polthier [1993] for discrete (or polyhedral) harmonic maps and minimal surfaces, Oberknapp and the second author developed an algorithm that defines a discrete version of Lawson's conjugate surface construction. We refer to [Oberknapp and Polthier 1997] and only point out two main ideas here.

Instead of minimizing the area functional the algorithm iterates the minimization of Dirichlet energy for discrete maps between discrete surfaces in $\mathbb{S}^3$ and produces a sequence of harmonic maps. Their images converge rapidly to a discrete minimal surface in $\mathbb{S}^3$ provided no triangles degenerate. In a second step the algorithm defines a conjugation method for discrete harmonic maps similar to the conjugation of smooth harmonic maps. Applying the conjugation to the above sequence of discrete harmonic maps produces a sequence of so-called "conjugate" harmonic maps that map discrete surfaces in $\mathbb{S}^3$ to discrete surfaces in $\mathbb{R}^3$. The conjugation is exact on the discrete level. This fact is especially remarkable since in the smooth case the conjugation process uses C^1 information of the spherical minimal surface, which is of course not directly available for polyhedral surfaces. The images of the discrete conjugate harmonic maps converge to a discrete CMC surface in $\mathbb{R}^3$. An amazing result of the algorithm is that the boundary behaviour of the smooth case (Theorem 2.1(ii)) is fulfilled exactly by the discrete surfaces.

The resulting polyhedral surface is polygonal and not triangular. An interesting open problem is to give a discrete variational definition of "discrete CMC" for the above polygonal surfaces. We point out just one problem: a nonflat polygon can be filled in with surfaces in many ways, and thus the volume of a polygonal complex is not immediate. Since a variational characterization requires the notion of area and volume, it depends on the choice of surface. However, the characterizing property of the discrete surfaces the algorithm produces is that their spherical conjugates are discrete minimal surfaces in the sense that any variations of the vertices in $\mathbb{S}^3$ do not decrease area; this means Lawson's Theorem 2.1 can be taken as the definition of the discrete constant mean curvature, as could be done in the smooth case as well.

To apply the algorithm amounts to the following steps.

- Determine the angular information of the desired CMC patch with n planar geodesic boundary arcs. Guess n edge lengths and fix $n-3$ of these. Taking the remaining three lengths as an initial condition, a root finder then finds a closed spherical polygon Γ with n great circle arcs as boundary.
- Solve the Plateau problem for Γ. In our examples the Gauß curvature varies considerably within a patch. Therefore interactive local refinement of the triangulation is necessary in regions of high curvature.
- The conjugation algorithm transforms a discrete minimal surface in $\mathbb{S}^3$ into a euclidean CMC surface.
- Check periods of the resulting CMC surface. If necessary repeat the previous steps with a different set of $n-3$ fixed initial lengths.

The algorithm can also give information on nonexistence: when we try to adjust the $n-3$ lengths to obtain a surface with vanishing periods it can happen that we leave the range of existence for the boundary polygons.

The periods depend on the triangulation. Experiments have shown this dependence to be surprisingly weak [Oberknapp and Polthier 1997]. Even so, we took care to adaptively triangulate those surfaces for which the period problem leads to polygons close to the boundary of existence.

4. FORCES AND BALANCED GRAPHS

4A. Balancing of Forces

Kusner's balancing formula gives a necessary condition on CMC surfaces derived from the first variation formula for a CMC surface; see [Korevaar et al. 1992], for example. The formula applies in general to 1-cycles γ contained in a CMC surface M and their bounding 2-chains D. Here, we have in mind that γ is a curve running once around a neck and D is a disk capping the neck. Considering all necks attached to a bubble then gives a condition at each bubble of a CMC surface.

To state the formula, assume that a set $B \subset \mathbb{R}^3$ (we think of a bubble) is bounded by an embedded subset Ω of the CMC surface M as well as a finite number of disjoint disks $D_i \subset \mathbb{R}^3$. Each disk D_i is in turn bounded by a circle $\gamma_i \subset \partial\Omega$. We choose exterior normals ν_i to D_i and exterior conormals η_i to γ_i, i.e., η_i is a normal to γ_i tangent to Ω. Then the *force* associated to the neck is the vector

$$W_i = \int_{\gamma_i} \eta_i - 2\int_{D_i} \nu_i .$$

The force can be shown to depend only on the homology class of γ_i. The *balancing formula* for B now states that the forces of the adjacent necks are in equilibrium,

$$\sum_i W_i = 0. \tag{4.1}$$

If a disk D is contained in a plane then its normal is constant and $\int_D \nu = \text{area}(D)\,\nu$. Moreover, if the plane is a symmetry plane for the surface then the

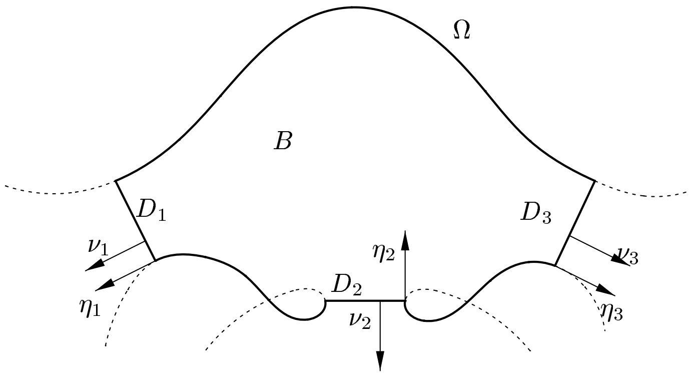

FIGURE 7. Notation for the balancing formula. For the bubble B the pull arising from the two lateral unduloidal necks is balanced by the force of the bottom nodoidal neck pushing the bubble upwards.

conormal is also constant and $\int_\gamma \eta = \text{length}(\gamma)\,\eta$ where $\eta = \pm\nu$. Thus we can express W in the form

$$W = (\pm\,\text{length}(\gamma) - 2\,\text{area}(D))\,\nu. \tag{4.2}$$

4B. Balanced Graphs

An edge graph can be associated to our surfaces and more general to a class of (not necessarily compact) CMC surfaces [Kusner 1991]. This class includes surfaces arising from special constructions, namely the symmetric Delaunay-like surfaces of Kapouleas or the first author, but excludes tori for instance. The picture to keep in mind is that each vertex of the graph represents a bubble, and each edge a single neck or a piece of a Delaunay surface comprising several necks. The graph is a topological retract of the surface and finite for compact CMC surfaces. Figure 3 gives an example.

Each edge of the graph associated to a neck is taken to be parallel to its force vector. Kusner [1991] chooses the line extending the edge as follows (Kapouleas' choice is different unless the surface is sufficiently symmetric). The homology class of a neck is assigned a *torque* $R_i(a) = \int_{\gamma_i} \eta \times (x-a) - 2\int_{D_i} \nu \times (x-a) \in \mathbb{R}^3$, which for given coordinates x depends on $a \in \mathbb{R}^3$. Then it can be checked that $|R_i(a)|$ attains its minimum on a line $\{a_0 + sW_i | s \in \mathbb{R}\}$; this is the line we want to define.

In general the set of these lines need not match in vertices, but in our case they do so by symmetry. Restricting the lines to the portion in between these intersection points gives a closed graph. Note that there is only one property of our graphs that is not immediate from symmetry: the length of the radial edges of our graphs. Thus scaling describes the only degree of freedom, and the minimization of torque in the above definition determines it.

For a closed graph there is an elegant way to express the balancing property. Label each edge of the graph associated to a CMC surface by a *weight* $w_i \in \mathbb{R}$ of the corresponding neck. We define w_i by $|w_i| = |W_i|$ and let its sign be positive if the force is outward (when calculated for the bubble at a bounding vertex), or negative, if it is inward. Note that viewed from the opposite vertex the normals η and ν change sign, so that inward and outward are well-defined. We will see below that by this definition unduloidal necks are assigned positive and nodoidal necks negative weights. Then for a given vertex the emanating edges e_i considered as outward directed vectors can be used to state the balancing formula in the form $\sum w_i e_i/|e_i| = 0$. A weighted graph with this property is called *balanced.*

From balancing many geometric properties of the graph follow. For instance if only two edges emanate from a vertex they must form a straight line, and we can omit the vertex. Thus the valence of each vertex can be assumed to be at least 3.

5. COMPARISON CMC SURFACES AND PRINCIPLES FOR EXISTENCE

We discuss two classes of noncompact surfaces that serve for us as comparison surfaces. We present these surfaces first and then draw conclusions in the form of heuristic principles for existence.

5A. Delaunay Surfaces

The *Delaunay surfaces* are the noncompact CMC surfaces of revolution. A meridian is generated by the trace made by the focus of an ellipse or hyperbola when these conical sections are rolled along a line. There are embedded *unduloids* and immersed *nodoids.* When normalized to mean curvature 1 each of them forms a one-parameter family of simply periodic surfaces.

The unduloid family ranges between the cylinder and a degenerate CMC surface, a string of spheres. One choice of parameter is the extreme radius of the meridian: the minimum is r and the maximum $1-r$ for the unduloids, with r running from 0 (string of spheres) to $1/2$ (cylinder). A different choice of parameter is the weight. For a neck of an unduloid (4.2) gives the weight

$$w_U = \text{length}(\gamma) - 2\,\text{area}(D) = 2\pi r(1-r) > 0,$$

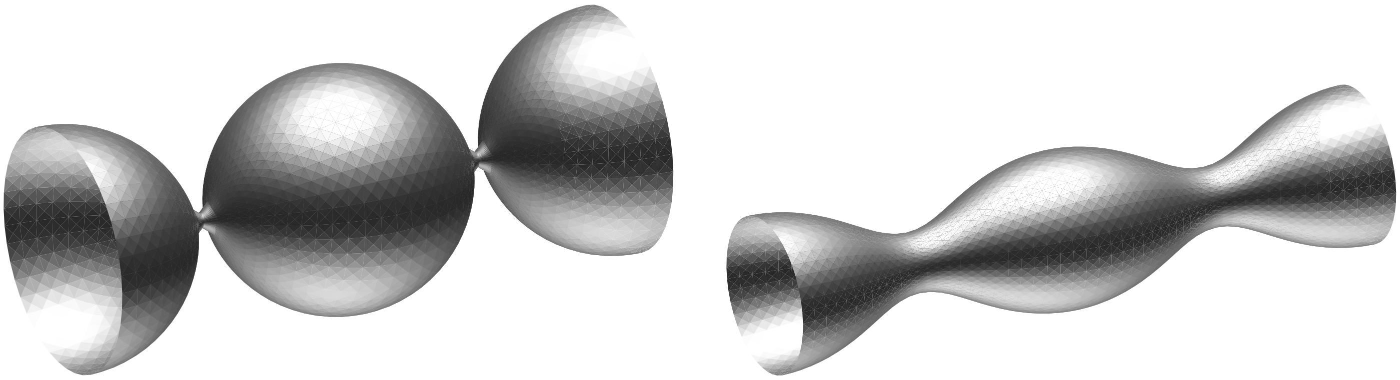

FIGURE 8. Necks of two Delaunay unduloids. As the unduloids deform from a chain of spheres to a cylinder, their period increases from 2 to π.

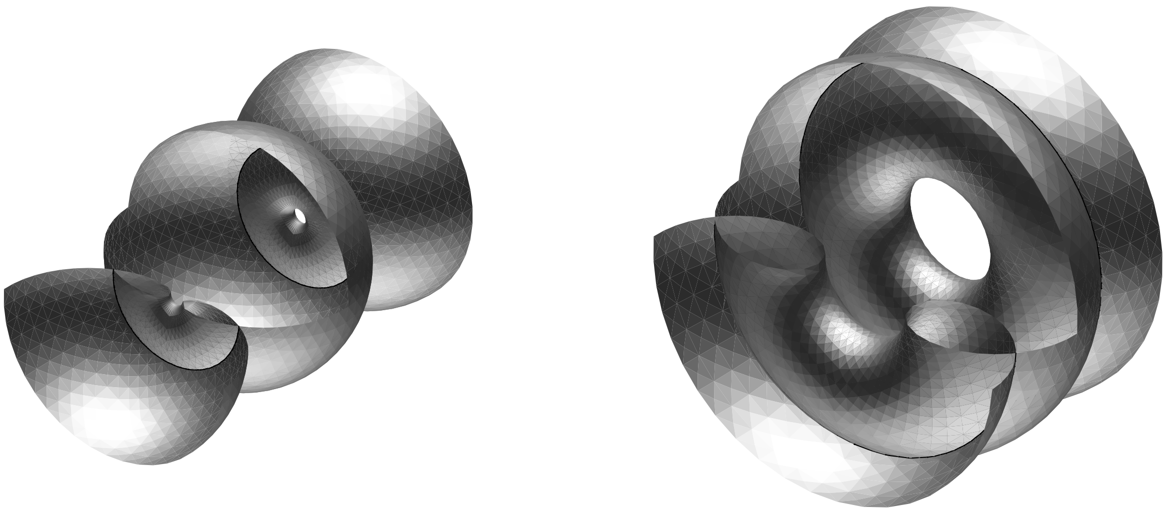

FIGURE 9. Necks of two Delaunay nodoids, partly cut open for clarity. As the nodoids increase in diameter the period decreases from 2 to 0.

where r is the radius of the circle $\gamma = \partial D$. Hence w_U decreases from $\pi/2$ for a cylinder to 0 for the spheres.

The family of nodoids can also be parameterized with the extreme radii: these are r and $1+r$ with $r \in \mathbb{R}_+$. When $r \to \infty$ the nodoids leave every fixed cylinder. The weights of nodoid necks

$$\begin{aligned} w_N &= -\operatorname{length}(\gamma) - 2\operatorname{area}(D) \\ &= -2\pi r(1+r) < 0 \end{aligned} \tag{5.1}$$

range from 0 (string of spheres) to $-\infty$. The period decreases from 2 for the sphere limit to 0 when r tends to infinity.

Figure 10 gives the one-to-one correspondence of Delaunay periods and weights. The period can be considered the edge length of the balanced graph of a Delaunay surface (with vertices located at each bubble).

5B. Dihedrally Symmetric k-Unduloids

These surfaces with symmetry group $D_k \times \mathbb{Z}_2$ have k ends whose asymptotic axes are contained in a plane and make an equal angle with one another. The dihedrally symmetric k-unduloids provide an example that not all weights satisfying the balancing formula do actually occur.

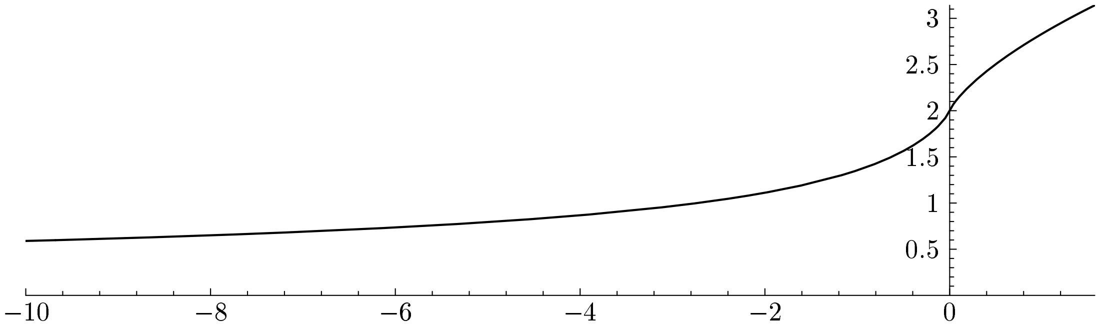

FIGURE 10. Period of the Delaunay surfaces as a function of the weight. The immersed nodoids have negative weights $-\infty < w < 0$ and periods tending to 0 with $w \to -\infty$. The embedded unduloids have positive weights $0 < w < \pi/2$, and periods ranging from 2 to π. The maximal weight $\pi/2$ is attained by the cylinder. Weight 0 can be attributed to a degenerate Delaunay surface, a chain of unit spheres. Figure courtesy of M. Heil.

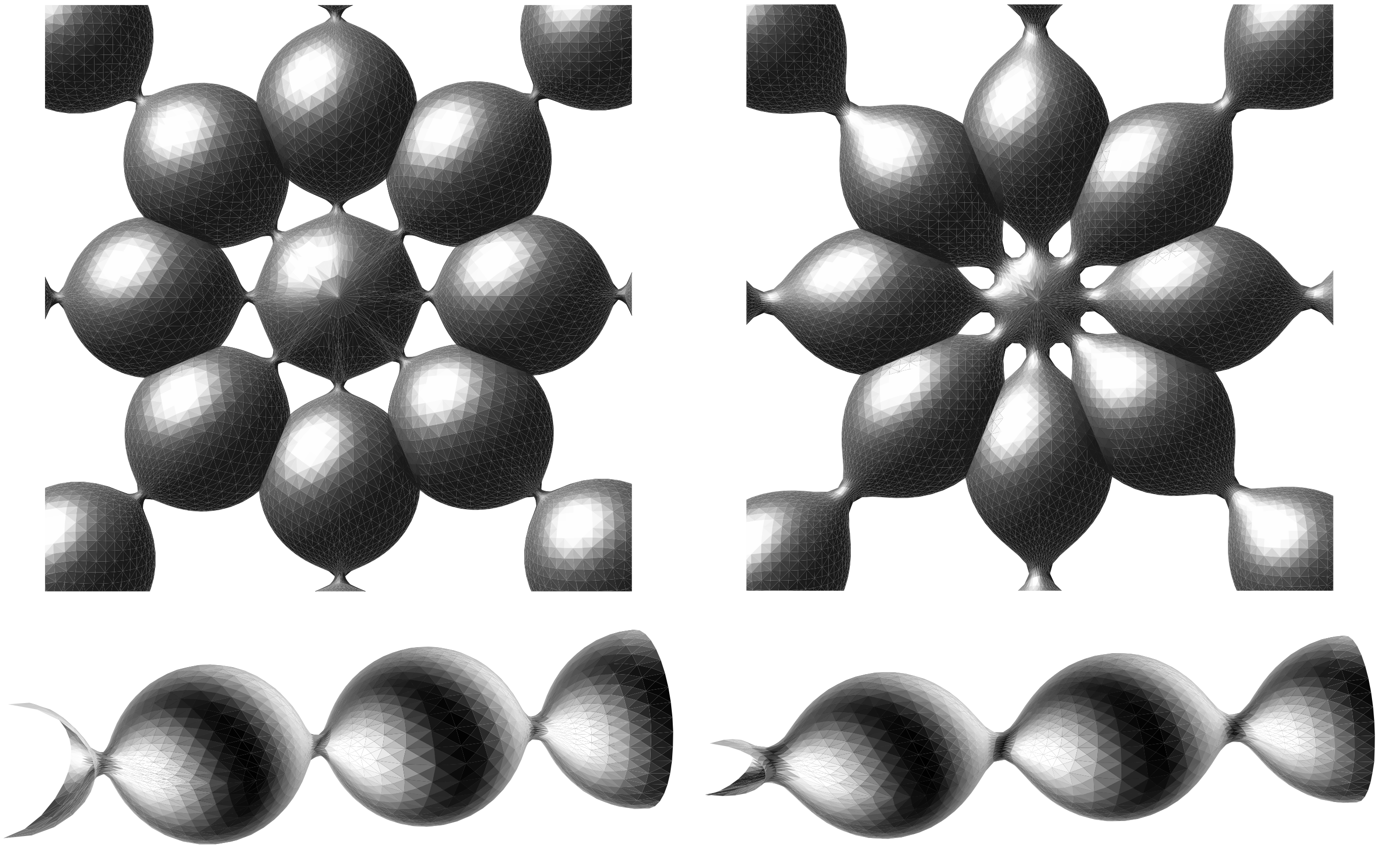

FIGURE 11. Noncompact dihedrally symmetric 8-unduloids of genus 0. The 8 ends are asymptotic to unduloids and their first bubbles intersect. The central bubble is spheroidal for the surface on the left and noidal for the one on the right. Existence of these surfaces is proved in [Große-Brauckmann 1993]. Bottom: Side view of the first bubbles of one end, including an eighth of the central bubble.

Theorem 5.1 [Große-Brauckmann 1993]. *There is a continuous one-parameter family of dihedrally symmetric k-unduloids for $k \geq 3$. Their ends are asymptotic to Delaunay unduloids. The family has one dihedrally symmetric k-unduloid with ends of weight $w_{\max}(k) := 2\pi(k-1)/k^2$ and two for each weight w with $0 < w < w_{\max}(k)$.*

How do the surfaces look like as we run through the entire one-parameter family? The ends deform from rays of spheres (weight 0) to unduloids with some maximal neck size (given by $w_{\max}(k)$) and again back to spheres (weight 0). The central sphere of the surface at one end of the family, which shown on the left in Figure 11, shrinks away over the family. Thus, at the other end of the family the k chains of spheres touch with their first sphere at the origin (the surface depicted on the right in Figure 11 is still somewhat away from this situation). To distinguish the two surfaces of the same weight we call the former part of the family *spheroidal* and the latter *noidal*. The term noidal is justified by a blow up of the surfaces close to the degenerate limit. If this blow up is done at the right rate the centre of the surfaces converges to a dihedrally symmetric minimal surface with k catenoid ends, the *k-noid*. This also holds for $k = 2$ when the limit of small unduloid necks is a standard catenoid.

The maximal weight $w_{\max}(k)$ corresponds to a maximal asymptotic neck radius $1/k$. Note that its decay in k leaves enough room to attach the first necks of the ends at the central sphere; for a slower growth the necks would interfere and new neck shapes would have to develop for large k.

5C. Construction Principles

The following heuristic principles guide our search for balanced graphs and their CMC surfaces.

(i) Weights and lengths are related similar to the Delaunay case (Figure 10).
(ii) An edge longer than 2 (but shorter than $\approx \pi$) is represented by an unduloid neck. If the length is larger than 4 we can take two unduloid necks enclosing an unduloid bubble, etc.
(iii) Edges of length less than 2 are represented by nodoidal necks. Again additional bubbles could be inserted for lengths less than integer multiples of 2.
(iv) The weights resulting from the lengths must be compatible with the balancing formula (4.1).

We note that (ii) and (iii) are a consequence of (i). We will also see that these two principles must be relaxed somewhat: in Section 6B we will represent edges longer than 1 by an unduloid neck. At each vertex the balancing condition (iv) imposes effectively one constraint on the weights and therefore on the lengths of the emanating edges.

Similar to the Delaunay comparison principle (i) we want to include a comparison for dihedrally symmetric necks to our list.

(v) The radial weight of a dihedrally symmetric k-fold neck is at most $\approx w_{\max}(k)$.

Without the symmetry assumption it is unclear which range of weights one should expect. For somewhat less symmetric situations this problem is studied in [Große-Brauckmann and Kusner 1996; Große-Brauckmann and Polthier 1997].

We draw an important conclusion. Suppose all edges at a vertex point into a half-space. This holds, for example, on the exterior vertices of a finite graph. Then (iii) implies that both unduloidal and nodoidal necks should be present. By (i) and (ii) edges of lengths both smaller and larger than 2 should emanate from the vertex. Similar conditions could be formulated if we have in mind to place k necks enclosing $k-1$ bubbles on an edge.

6. FAMILIES OF COMPACT SURFACES

We now want to apply the five guiding principles of the preceding section to the graphs of our compact surfaces. No further constraints are present. Principle (iv), the balancing formula, implies that the valence of each vertex is at least 3, so that the graph G_2 (see Section 1) does not arise from our construction.

We first consider the dihedrally symmetric case. For the midpoint of G_g the balancing formula (4.1) is satisfied by symmetry. Indeed g radial edges emanate from the central vertex and they all have the same (positive or negative) weight. For the outer vertices all edges point into a half-space and, as pointed out in Section 5C, the balancing formula implies that unduloidal and nodoidal necks should be present on the adjoining edges. Which distribution is appropriate depends on the length quotient q_g. The radial and polygonal edges enclose an angle π/g, so that by the balancing formula (4.1) the two polygonal weights $w_P(g)$ result in a radial weight $w_R(g)$

$$w_R(g) = -2\sin(\pi/g)w_P(g). \tag{6.1}$$

6A. Dihedrally Symmetric Spheroidal Surfaces

We regard $w_R(g)$ and $w_P(g)$ as functions of the lengths of G_g, with values approximately given by the Delaunay weights. We look for a scaling of the graph G_g such that the induced weights $w_R(g)$ and $w_P(g)$ satisfy (6.1). For $g = 6$ the degenerate weights $w_R = w_P = 0$ satisfy this equation, and the corresponding scaling of G_6 with edge length 2 is the graph for the degenerate surface consisting of 7 touching spheres.

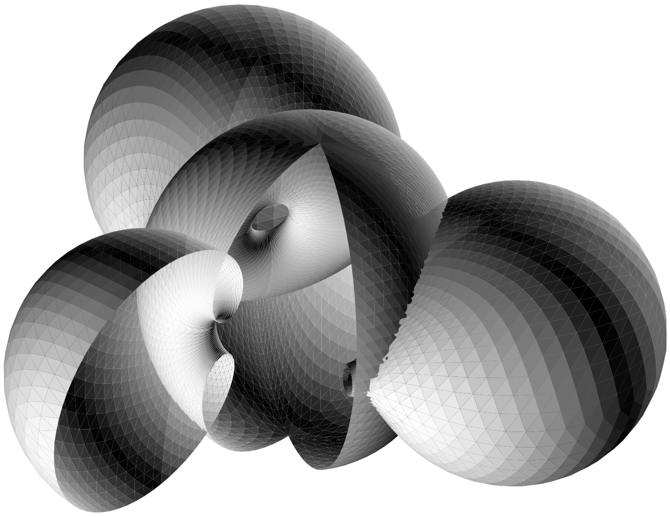

FIGURE 12. Spheroidal surface of genus 3. A sixth of the surface is removed. As the tetrahedral surface of Figure 2 the three unduloidal necks are contained in the central bubble (see the front end of the unduloidal bubble on the right).

For $3 \le g \le 5$ we have $q_g > 1$. Thus there is a scaling of the graph G_g with radial edges shorter than 2 and polygonal edges longer than 2. In view of principle (ii) and (iii) this suggests unduloidal necks on the polygonal edges and nodoidal necks on the spokes. Using the Delaunay comparison principle (i) we see the length of the spokes must be approximately in the interval $(2/q_g, 2)$: the left endpoint corresponds to polygonal edge length 2 so that the right hand side of (6.1) vanishes, whereas at the right endpoint the left hand side of (6.1) vanishes. Thus the actual length can be viewed to be the result of an intermediate value problem for (6.1).

Note that for the same radial edge length both $\sin(\pi/g)$ and, assuming principle (i), $w_P(g)$ are larger for $g = 3$ than for $g = 4$ and 5. Thus for (6.1) to hold the scaling of G_3 must be smallest. This gives the genus 3 surface the largest radial necks in agreement with our experimental results.

If $g > 6$ then $q_g < 1$, so that the polygonal edges of G_g are shorter than the spokes. To be consistent with principle (ii) and (iii) we need to flip unduloidal and nodoidal necks compared to the previous family. An intermediate value argument similar to the above gives that G_g with spokes of unit length has to be scaled with some factor in $(2, 2/q_g)$. We obtained existence for $g = 8, 9, 10$ with increasing neck sizes. For genus 7 the necks are thin and the surface is numerically harder to deal with our algorithm; on the other hand Kapouleas' theoretical existence result makes this surface most likely to exist. Therefore we skipped $g = 7$.

6B. Dihedrally Symmetric Noidal Surfaces

Similarly to the noidal and spheroidal dihedrally symmetric k-unduloids of the same weight (Section 5B) we obtain a further set of CMC surfaces with the same graphs G_g. These have a noidal central bubble and nodoidal polygonal necks. For this type there is only "half a neck" on each spoke but

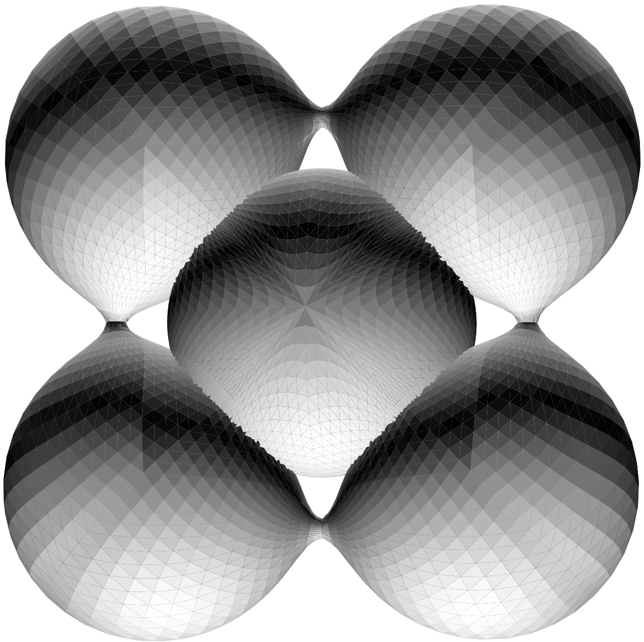

FIGURE 13. Spheroidal surface of genus 4. The outer bubbles are connected by unduloidal necks and in turn have nodoidal necks joining them to the central bubble. The outer bubbles look much like bent unduloids and, like these, they are flatter than the centre bubble.

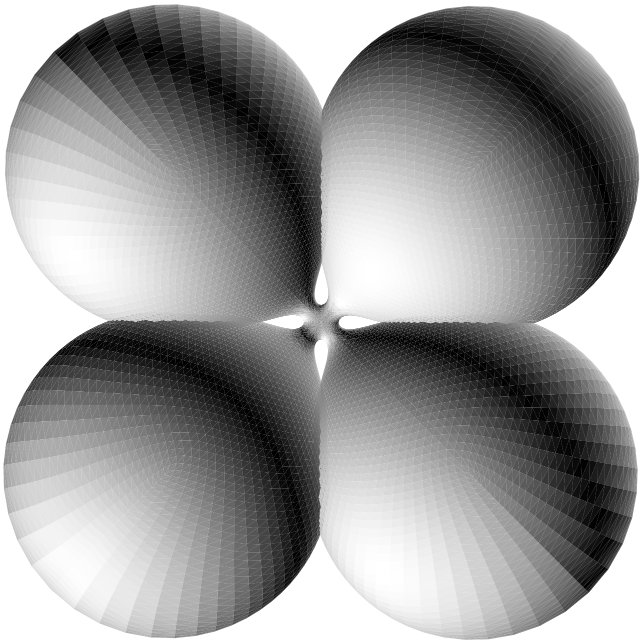

FIGURE 14. A noidal of genus 4. In this surface, nodoidal and unduloidal necks are flipped relative to the surface of Figure 13. This surface has a central 4-noidal neck. The outer bubbles are connected with nodoid necks, which are not visible in this view.

still an entire neck on each polygonal edge. The critical length quotient is therefore $q_g = 1/(1/2) = 2$. The difference $2 - q_g$ is always positive (for $g \geq 3$), and by principle (i) we must have unduloidal spokes and nodoidal polygonal necks for all $g \geq 3$.

Our experiments covered genus 4, 5, 8, and 9; we skipped genus 6 and 7 because in view of principle (v) existence is clear to us from the existence of the higher genera. In [Große-Brauckmann and Polthier 1996] we mentioned the numerical complications we faced when we tried to solve the period problem for the surface with $g = 3$, so that we did not have enough experimental evidence to claim existence of the surface. However, in view of the existence of similar surfaces with larger genus (and larger necks) we do not doubt existence for genus 3 any more. This is in agreement with principle (v): for large, not for small neck sizes, existence is problematic.

How are the neck sizes of a spheroidal and noidal surface related, for the common genera 7 to 9? Clearly the scaling of the noidal graph is smaller. This makes the polygonal lengths of the noidal surfaces larger so that the nodoidal necks are larger. By (6.1) the unduloidal necks must be larger too.

6C. Finiteness of the Dihedrally Symmetric Families

The key to understanding the upper limit $g = 10$ of the spheroidal family is to see how the radial weight grows in the genus. Unlike the spheroidal case for $g = 3, 4, 5$ an estimate of the radial forces is not straightforward from (6.1); indeed with increasing genus $\sin(\pi/g)$ decreases, whereas the nodoidal weights $|w_P(g)|$ increase for shorter edges according to principle (i). Hence it is not clear how the resulting weight $-2\sin(\pi/g)w_P(g)$ depends on g; it could still be bounded for $g \to \infty$.

We now give an estimate for $-2\sin(\pi/g)w_P(g)$ based on the Delaunay comparison principle (i).

genus g	weight of a Delaunay nodoid with period $2q_g$ (cf. Figure 10)	resulting radial weight assuming (6.1)	approximate experimental radial weight	max. weight $w_{\max}(k)$ of a dihedrally symmetric k-unduloid
7	-0.23	0.20	(—)	0.77
8	-0.57	0.43	0.18	0.69
9	-0.96	0.62	0.29	0.62
10	-1.2	0.87	0.43	0.57
15	-4.4	1.8	—	0.39
20	-8.6	2.7	—	0.30
100	-248	16	—	0.06
500	-6700	84	—	0.01

TABLE 3. Weight comparison for the dihedrally symmetric surfaces.

To simplify we assume that after scaling the graph has spokes of length 2. This gives the polygonal edge a length $2q_g = 4\sin(\pi/g)$, i.e., we consider one of the limiting cases of the intermediate value argument of 6A. In Table 3 we list the weight of a Delaunay nodoid with period $2q_g$. The values of w_P resulting from (6.1) are unbounded. However, from the Delaunay comparison we expect an upper bound for the weight and thus only finitely many compact surfaces of the considered type should exist.

More specifically, by principle (v) the weights should be no larger than approximately $w_{\max}(k)$. This holds up to genus 9, which is in good coincidence with our experimentally determined limiting genus 10. We note that in fact the actual lengths of the graphs are larger, so that the weights are smaller than the estimate given in Table 3. For comparison we computed approximate experimental weights by assuming that the polyhedral neck cross section is a circle of the length stated in Table 1, for which (5.1) gives the weight. The resulting weights are experimental evidence for (v): up to genus 10 they are well below $w_{\max}(10)$, but for genus 11 the weight expected from linear extrapolation would be larger than $w_{\max}(11)$.

How does the limitation in genus appear in our experiments? We can still find fundamental domains for higher genus, but we cannot close the periods. The reason for this is that the range of existence for the boundary polygons is limited. This range can be determined using spherical trigonometric formulas. For genus 10 we are well away from the boundary of existence and for genus 11 the periods for existing domains are sufficiently large to give us confidence that smooth CMC surfaces also exist exactly up to (and including) 10.

We can also explain why the maximal genus 9 of the noidal surfaces is smaller than the maximal genus 10 of the spheroidal family. As we pointed out in Section 6B, the neck sizes of the noidal surfaces are larger than those of the spheroidal surfaces. Consequently the noidal surfaces reach the limiting weight $\approx w_{\max}(k)$ for a lower genus than the spheroidal ones.

6D. Platonic Symmetry

The value for the length quotient listed in Table 2 suggests four spheroidal surfaces with unduloidal polyhedral necks and nodoidal radial necks, and our experiments gave existence for all these cases. The dodecahedron has length quotient less than 1 and we expect a surface of genus 30 with 20 outer bubbles with polyhedral nodoidal necks. We did not investigate this surface but its existence seems very likely.

Similar to the dihedrally symmetric case there is a noidal family. The length quotient for the dodecahedral surface is so far away from 2 that the radial necks must be too large to exist—this explains why we could not close the periods for the dodecahedral surface. However, the icosahedral and cubic

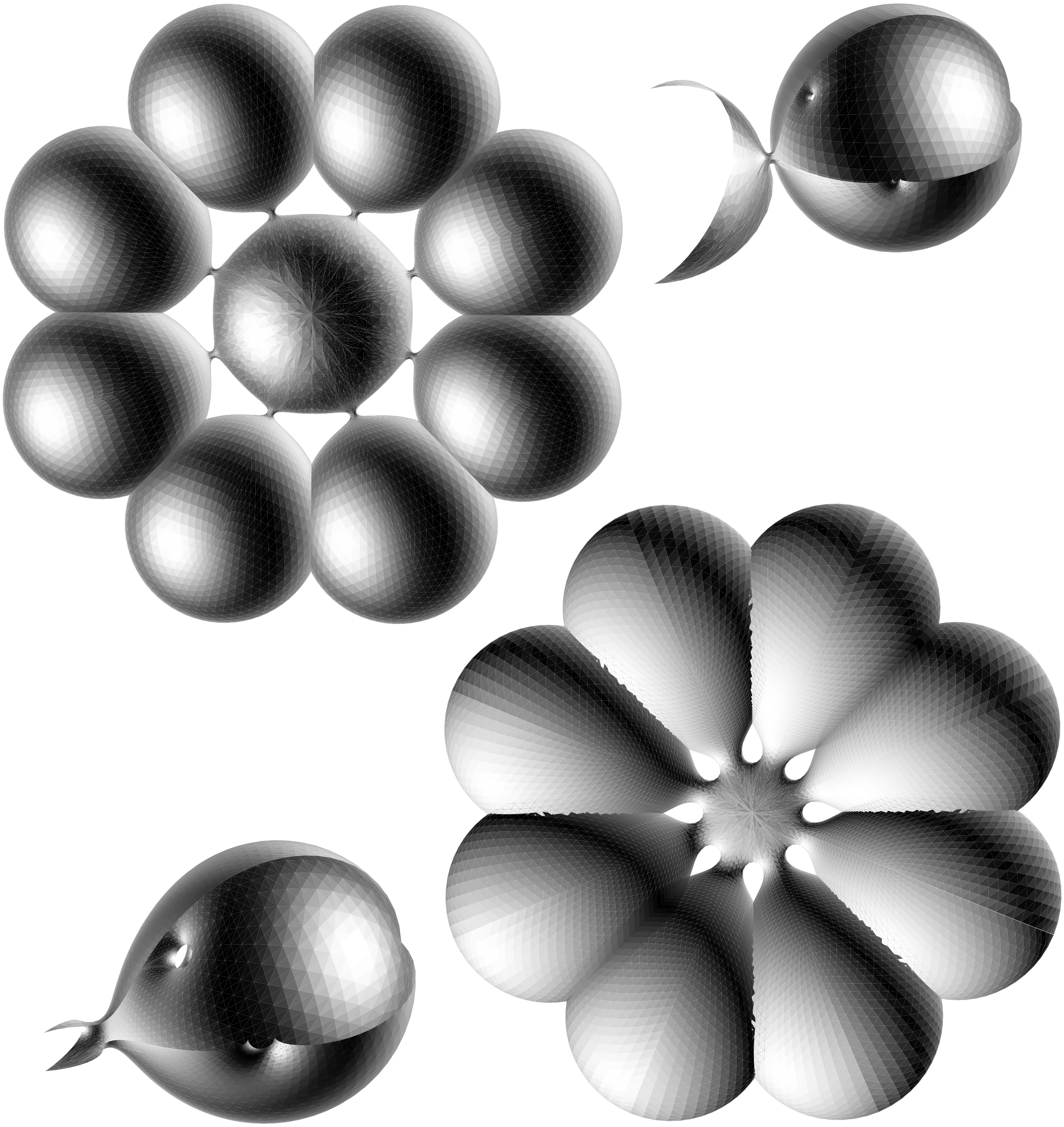

FIGURE 15. Two surfaces of genus 8. In both the outer bubbles are connected with nodoidal necks. However, the spheroidal surface on the top has a much larger central bubble than the noidal surface on the bottom. The details show three fundamental domains and give view to the nodoidal necks. Compare this figure to the two 8-unduloids of Figure 11.

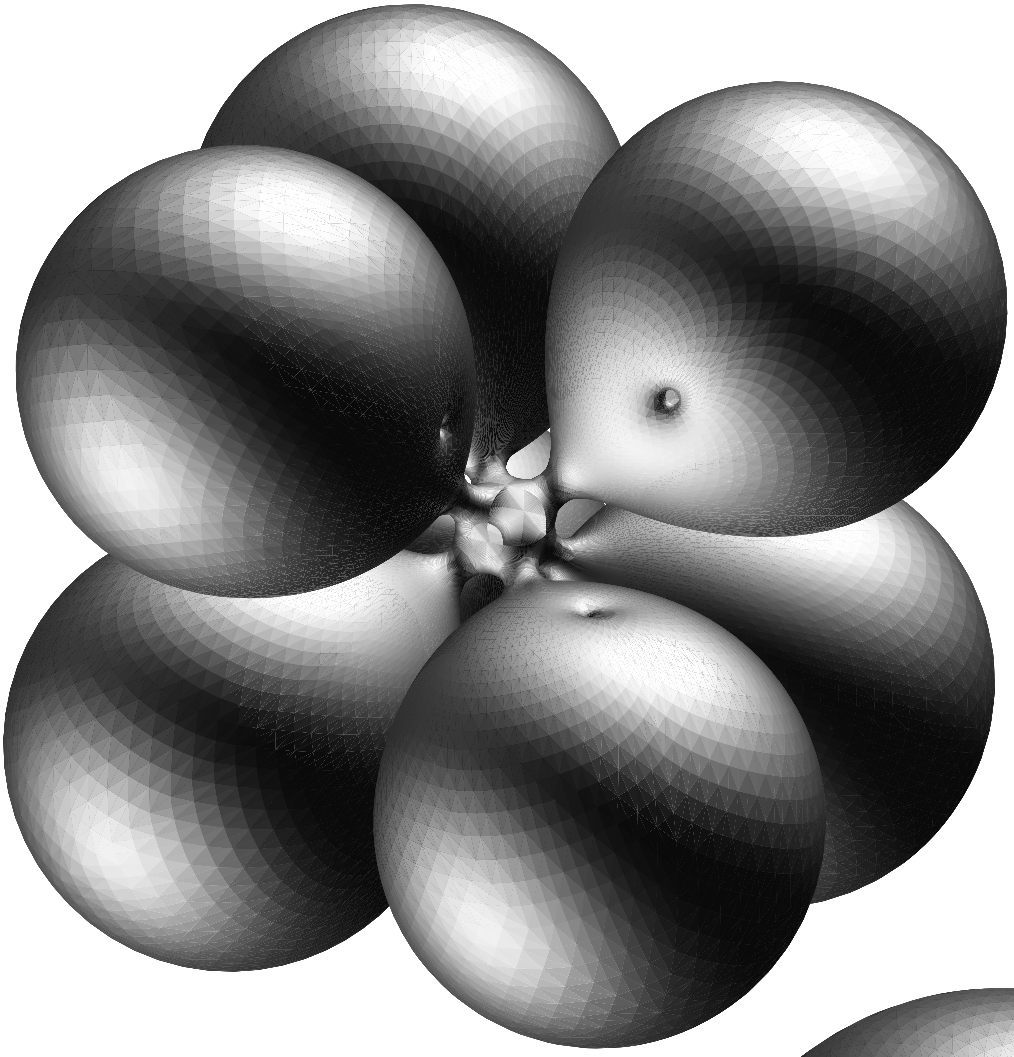

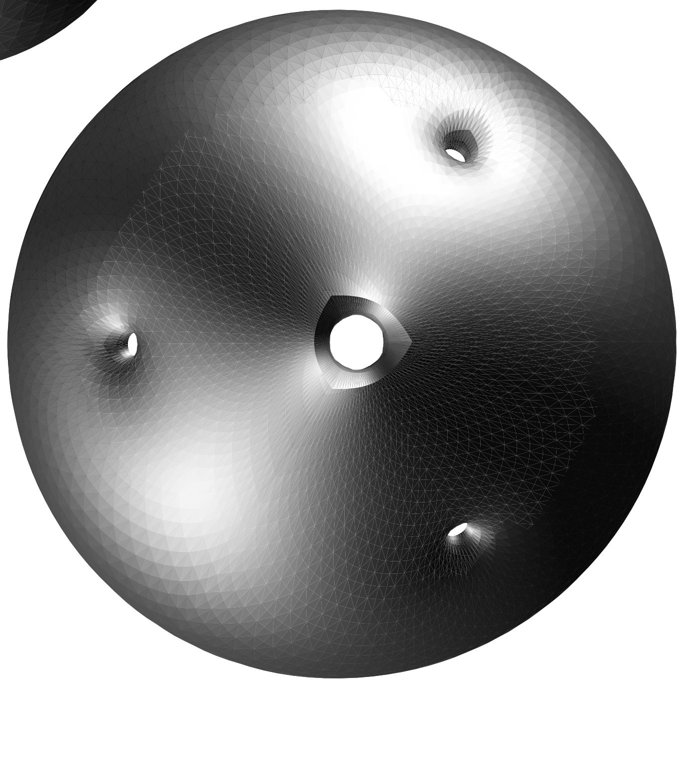

FIGURE 16. Noidal surface of genus 12 with cubical symmetry. Top: One bubble is removed to give a view of the centre of the surface, which resembles an 8-ended catenoid. Bottom: One bubble, viewed from the centre.

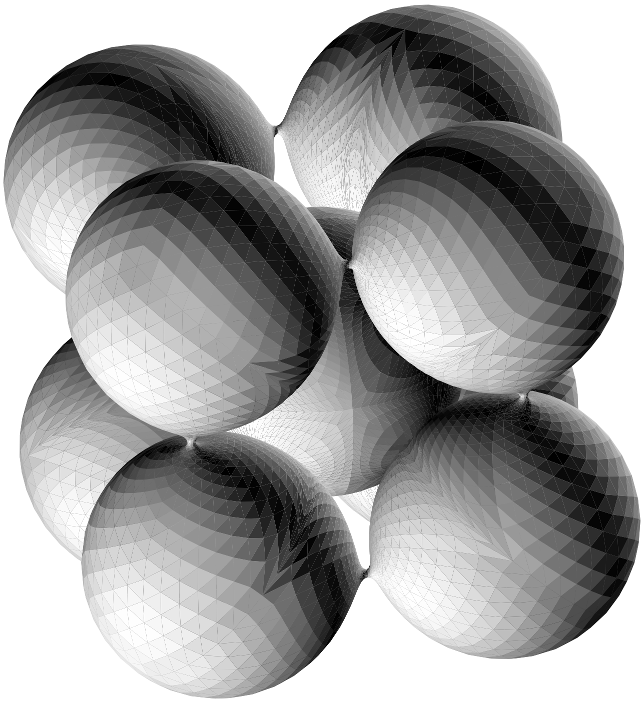

FIGURE 17. Spheroidal surface of genus 12 with cubical symmetry.

surfaces exist. In view of (v) we are confident that this implies existence for the surfaces with smaller weights: these are the surfaces with tetrahedral and octahedral graph and symmetry.

7. FURTHER CLASSES

We mention a few classes of graphs that could admit similar compact CMC surfaces. We choose examples that are symmetric enough for our construction to be applicable. Figure 18.1 shows a square whose opposite vertices are joined by two further edges (no vertex at the centre). Similarly, a regular $2k$-gon ($k \geq 2$) whose opposite vertices are joined gives a graph with dihedral symmetry $D_{2k} \times \mathbb{Z}_2$; the corresponding CMC surfaces would have genus $k+1$. Figure 18.2 shows a different way to connect the vertices of G_6: while the spokes are kept every other hexagon point is joined. Similarly $g+1$ points ($g \geq 5$) give a graph with symmetry $D_g \times \mathbb{Z}_2$, for candidate surfaces of genus g. Instead of every other polygonal vertex, we could join every third, fourth, etc., so there are further similar families. In Figure 18.3 the modification of G_6 is opposite: the polygonal edges of G_6 are kept, but there are two different vertices in the centre, each one joined to every other polygonal vertex. More generally, a $2k$-gon gives a graph of symmetry $D_{2k} \times \mathbb{Z}_2$ for surfaces of genus $2k-1$; again there are similar families with further central vertices. Other options that might soon leave the limits of our construction are to increase the number of bubbles, or to decrease symmetry.

There are many beautiful graphs with Platonic symmetry, some of which lead to further compact CMC surfaces. A description of these graphs is rather tedious, and we leave the pleasure of finding them to the reader.

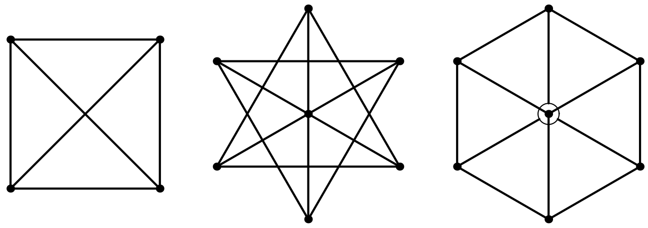

FIGURE 18. More planar graphs with dihedral symmetry.

REFERENCES

[Aleksandrov 1958] A. D. Aleksandrov, "Uniqueness theorems for surfaces in the large. V", *Amer. Math. Soc. Transl.* (2) **21** (1962), 412–416. Translated from *Vestnik Leningrad. Univ.* **13**:19 (1958), 5–8.

[Barbosa and do Carmo 1984] J. L. Barbosa and M. do Carmo, "Stability of hypersurfaces with constant mean curvature", *Math. Z.* **185** (1984), 339–353.

[Bobenko 1991] A. I. Bobenko, "All constant mean curvature tori in $\mathbb{R}^3$, S^3, H^3 in terms of theta-functions", *Math. Ann.* **290**:2 (1991), 209–245.

[Brakke 1992] K. A. Brakke, "The surface evolver", *Experiment. Math.* **1**:2 (1992), 141–165.

[Delaunay 1841] C. Delaunay, "Sur la surface de révolution, dont la courbure moyenne est constante", *J. de mathématiques* **6** (1841), 309–320.

[Ercolani et al. 1993] N. M. Ercolani, H. Knörrer, and E. Trubowitz, "Hyperelliptic curves that generate constant mean curvature tori in $\mathbb{R}^3$", pp. 81–114 in *Integrable systems* (Luminy, 1991), Progr. Math. **115**, Birkhäuser, Boston, MA, 1993.

[Große-Brauckmann 1993] K. Große-Brauckmann, "New surfaces of constant mean curvature", *Math. Z.* **214**:4 (1993), 527–565.

[Große-Brauckmann 1997] K. Große-Brauckmann, "Gyroids of constant mean curvature", *Experiment. Math.* **6** (1997), 21–38.

[Große-Brauckmann and Kusner 1996] K. Große-Brauckmann and R. Kusner, "Moduli spaces of embedded constant mean curvature surfaces with few ends and special symmetry", preprint, SFB 256, Universität Bonn, 1996.

[Große-Brauckmann and Polthier 1996] K. Große-Brauckmann and K. Polthier, "Numerical examples of compact surfaces of constant mean curvature", pp. 23–46 in *Elliptic and parabolic methods in geometry*, edited by B. Chow et al., A K Peters, Wellesley, MA, 1996.

[Große-Brauckmann and Polthier 1997] K. Große-Brauckmann and K. Polthier, "Constant mean curvature surfaces derived from Delaunay's and Wente's examples", pp. 119–134 in *Visualization and mathematics*, edited by H.-C. Hege and K. Polthier, Springer, Heidelberg, 1997.

[Heil 1995] M. Heil, *Numerical tools for the study of finite gap solutions of integrable systems*, Ph.D. thesis, Technische Universität Berlin, 1995.

[Hopf 1983] H. Hopf, *Differential geometry in the large*, Lecture Notes in Mathematics **1000**, Springer, Berlin, 1983.

[Kapouleas 1991] N. Kapouleas, "Compact constant mean curvature surfaces in Euclidean three-space", *J. Differential Geom.* **33**:3 (1991), 683–715.

[Kapouleas 1995] N. Kapouleas, "Constant mean curvature surfaces constructed by fusing Wente tori", *Invent. Math.* **119**:3 (1995), 443–518.

[Karcher 1989] H. Karcher, "The triply periodic minimal surfaces of Alan Schoen and their constant mean curvature companions", *Manuscripta Math.* **64**:3 (1989), 291–357.

[Korevaar et al. 1992] N. J. Korevaar, R. Kusner, W. H. Meeks, III, and B. Solomon, "Constant mean curvature surfaces in hyperbolic space", *Amer. J. Math.* **114**:1 (1992), 1–43.

[Kusner 1991] R. Kusner, "Bubbles, conservation laws, and balanced diagrams", pp. 103–108 in *Geometric analysis and computer graphics* (Berkeley, CA, 1988), Math. Sci. Res. Inst. Publ. **17**, Springer, New York, 1991.

[Lawson 1970] H. B. Lawson, Jr., "Complete minimal surfaces in S^3", *Ann. of Math.* (2) **92** (1970), 335–374.

[Oberknapp and Polthier 1997] B. Oberknapp and K. Polthier, "An algorithm for discrete constant mean curvature surfaces", pp. 141–161 in *Visualization and mathematics*, edited by H.-C. Hege and K. Polthier, Springer, Heidelberg, 1997.

[Pinkall and Polthier 1993] U. Pinkall and K. Polthier, "Computing discrete minimal surfaces and their conjugates", *Experiment. Math.* **2**:1 (1993), 15–36.

[Pinkall and Sterling 1989] U. Pinkall and I. Sterling, "On the classification of constant mean curvature tori", *Ann. of Math.* (2) **130**:2 (1989), 407–451.

[Wente 1986] H. C. Wente, "Counterexample to a conjecture of H. Hopf", *Pacific J. Math.* **121**:1 (1986), 193–243.

Karsten Große-Brauckmann, Universität Bonn, Mathematisches Institut, Beringstraße 1, 53115 Bonn, Germany (kgb@math.uni-bonn.de)

Konrad Polthier, Technische Universität Berlin, Fachbereich Mathematik, MA 8-3, Straße des 17. Juni 136, 10623 Berlin, Germany (polthier@math.tu-berlin.de)

Received October 30, 1995; accepted in revised form October 2, 1996